Electronic charge and spin density distribution in a quantum ring with spin-orbit and Coulomb interactions

Csaba Daday,[1,2] Andrei Manolescu,[1] D. C. Marinescu,[3] and Vidar Gudmundsson[2]
[1]*School of Science and Engineering, Reykjavik University, Menntavegur 1, IS-101 Reykjavik, Iceland*
[2]*Science Institute, University of Iceland, Dunhaga 3, IS-107 Reykjavik, Iceland*
[3]*Department of Physics and Astronomy, Clemson University, Clemson, South Carolina 29621, USA*
(Received 18 June 2011; published 20 September 2011)

Charge and spin density distributions are studied within a nanoring structure endowed with Rashba and Dresselhaus spin-orbit interactions (SOIs). For a small number of electrons, in the presence of an external magnetic field and of the Coulomb interaction, the energy spectrum of the system is calculated through an exact numerical diagonalization procedure. The eigenstates thus determined are used to estimate the charge and spin densities around the ring. We find that when more than two electrons are considered, the charge density deformations induced by SOIs are dramatically flattened by the Coulomb repulsion, while the spin density deformations are amplified.

DOI: 10.1103/PhysRevB.84.115311 PACS number(s): 71.70.Ej, 73.21.Hb, 71.45.Lr

I. INTRODUCTION

The possibility of controlling the flow of the electron spins in semiconductor structures by external electric means through spin-orbit interactions (SOIs) has dominated the recent past of spintronics research. This fundamental principle, first explored in the Datta-Das spin transistor configuration,[1] has been guiding a sustained effort to understand all the phenomenological implications of SOI for electron systems. The coupling between spin and orbital motion results either from the two-dimensional confinement[2] (Rashba) or from the inversion asymmetry of the bulk crystal structure[3] (Dresselhaus). The usual expression of the the spin-orbit Hamiltonian H_{SO} retains only the linear terms in the electron momentum $\mathbf{p} = (p_x, p_y)$ and is given by

$$H_{SO} = \frac{\alpha}{\hbar}(\sigma_x p_y - \sigma_y p_x) + \frac{\beta}{\hbar}(\sigma_x p_x - \sigma_y p_y). \qquad (1)$$

The Rashba and Dresselhaus coupling constants are α and β, respectively, while $\sigma_{x,y,z}$ are the Pauli matrices. In general, the two interactions are simultaneously present and often have comparable strengths. While α, the coupling constant of the Rashba interaction, can be modified by external electric fields induced by external gates, the strength of the Dresselhaus SOI, β, is fixed by the crystal structure and by the thickness of the quasi-two-dimensional electron system.[4,5] In many situations of interest, an additional energy scale is introduced by the Zeeman interaction of the electron spin with an external magnetic field, proportional to the effective gyromagnetic factor g^*, which depends on the material energy-band structure. While $g^* = -0.44$ is very small in GaAs, it can be more that 100 times larger in InSb.

The interplay between the two types of SOI, which have competing effects on the precession of the electron spin as they rotate it in opposite directions, and the Zeeman splitting, which minimizes the energy by aligning the spin parallel to the external field, determines the ground-state polarization of the electron system and the characteristics of spin transport. The investigation of such problems in mesoscopic rings has been pursued intensively by several authors.[6–10] In particular, it was noticed that, in the absence of the Coulomb interaction among the electrons, the interference between the Rashba and Dresselhaus precessions relative to the orbital motion leads to the creation of an inhomogeneous spin and charge distribution around the ring.[8] The charge inhomogeneity created in this situation has a symmetric structure with two maxima and two minima around the ring and will be called here a charge density deformation (CDD). The effect of the Coulomb interaction on this type of charge distribution has been considered for two electrons. The result was obtained that, on account of the electrostatic repulsion, the two electrons become even more localized in the potential minima associated with the CDD, leading to an amplitude increase.[9,10]

In this work we obtain an estimate of the effect of the Coulomb interaction on the charge and spin distributions associated with $N = 2$, 3, and 4 electrons in a ring with SOI coupling by an exact diagonalization procedure that uses the configuration-interaction method. Our results indicate that, when the number of electrons increases, the mutual repulsion leads to more uniform charge distribution around the ring, generating a dramatically flattened CDD. In contrast, the spin density deformation (SDD) is amplified by the Coulomb effects. This can be explained by the appearance of a stronger repulsion between same spin electrons, leading to more favorable spin orientations.

II. THE RING MODEL

The system of interest in our problem is a two-dimensional quantum ring of exterior and interior radii R_{ext} and R_{int}, respectively. The ring is placed in a perpendicular magnetic field B associated in the symmetric gauge with a vector potential $\mathbf{A} = (B/2)(-y,x,0)$. The single-particle Hamiltonian of an electron of momentum $\mathbf{p} = -i\hbar\nabla + e\mathbf{A}$ and effective mass m^* is written as the sum of an orbital term $H_O = \mathbf{p}^2/2m^*$, a Zeeman contribution $H_Z = (1/2)g^*\mu_B B\sigma_z$, and the spin-orbit coupling given in Eq. (1). The ensuing expression,

$$H = H_O + H_Z + H_{SO}, \qquad (2)$$

 ©2011 American Physical Society

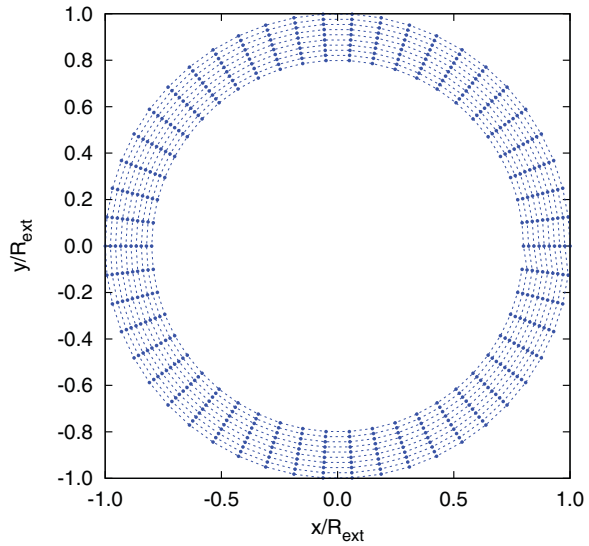

FIG. 1. (Color online) The discretized ring with $R_{\rm int} = 0.8R_{\rm ext}$, and 10 radial × 50 angular sites. The sites are shown as circular points. The thin dotted lines connecting sites are for guiding the eye.

is discretized in a standard manner[6,7,11] on a grid[12] defined by N_r radial and N_φ angular sites, as shown in Fig. 1. The radial coordinate of each site is $r_k = R_{\rm ext} - (k-1)\delta r$, with $k = 1,2,\ldots,N_r$, while $\delta r = (R_{\rm ext} - R_{\rm int})/(N_r - 1)$ is the distance between adjacent sites with the same angle. Similarly, the angular coordinate is $\varphi_j = (j-1)\delta\varphi$, where $j = 1,2,\ldots,N_\varphi$ and $\delta\varphi = 2\pi/N_\varphi$ is the angle between consecutive sites with the same radius. The Hilbert space is spanned by the ket vectors $|kj\sigma\rangle$, where the first integer, k, stands for the radial coordinate, the second one, j, for the angular coordinate, and $\sigma = \pm 1$ denotes the spin projection in the z direction.

In this basis $\{|kj\sigma\rangle\}$, the matrix elements of the orbital Hamiltonian are given by

$$\langle kj\sigma|H_O|k'j'\sigma'\rangle = T\delta_{\sigma\sigma'}\left\{\left[t_\varphi + t_r + \frac{1}{2}t_B^2\left(\frac{r_k}{4R_{\rm ext}}\right)^2\right]\delta_{kk'}\delta_{jj'} - \left[t_\varphi + t_B\frac{i}{4\delta\varphi}\right]\delta_{kk'}\delta_{jj'+1} + t_r\delta_{kk'+1}\delta_{jj'}\right\} + \text{H.c.} \quad (3)$$

$T = \hbar^2/(2m^*R_{\rm ext}^2)$ is the energy unit, while $R_{\rm ext}$ is the length unit. In T units, we obtain $t_\varphi = [R_{\rm ext}/(r_k\delta\varphi)]^2$ for the angular hopping energy, $t_r = (R_{\rm ext}/\delta r)^2$ for the radial hopping energy, and $t_B = \hbar eB/(m^*T)$ for the magnetic cyclotron energy. (H.c. denotes the Hermitian conjugate.)

In the same basis, the Zeeman Hamiltonian is simply diagonal in the spatial coordinates,

$$\langle kj\sigma|H_Z|k'j'\sigma'\rangle = \tfrac{1}{2}Tt_B\gamma(\sigma_z)_{\sigma\sigma'}\delta_{kk'}\delta_{jj'}, \quad (4)$$

where $\gamma = g^*m^*/(2m_e)$ is the ratio between the Zeeman gap and the cyclotron energy, m_e being the free-electron mass.

For the spin-orbit Hamiltonian we obtain

$$\langle kj\sigma|H_{SO}|k'j'\sigma'\rangle = \frac{1}{2}Tt_\alpha\left[t_B\frac{r_k}{4R_{\rm ext}}\left(\sigma_r^j\right)_{\sigma\sigma'}\delta_{kk'}\delta_{jj'} + it_\varphi^{1/2}\frac{\left(\sigma_r^j+\sigma_r^{j+1}\right)_{\sigma\sigma'}}{2}\delta_{kk'}\delta_{jj'+1} - it_r^{1/2}\left(\sigma_\varphi^j\right)_{\sigma\sigma'}\delta_{kk'+1}\delta_{jj'}\right] + Tt_\beta\sum_{k,j}\left[\sigma_r^j \to \left(\sigma_\varphi^j\right)^* \text{ and } \sigma_\varphi^j \to -\left(\sigma_r^j\right)^*\right] + \text{H.c.}, \quad (5)$$

where $t_\alpha = \alpha/(R_{\rm ext}T)$ and $t_\beta = \beta/(R_{\rm ext}T)$ are the two types of spin-orbit relative energy, while $\sigma_r(\varphi) = \sigma_x\cos\varphi + \sigma_y\sin\varphi$ and $\sigma_\varphi(\varphi) = -\sigma_x\sin\varphi + \sigma_y\cos\varphi$ are the radial and angular Pauli matrices, respectively. We used the slightly shorter notations $\sigma_r^j = \sigma_r(\varphi_j)$ and $\sigma_\varphi^j = \sigma_\varphi(\varphi_j)$ for the matrices at the particular angles on our lattice. The Rashba spin-orbit terms are all included in the first square brackets. The Dresselhaus terms are very similar to the Rashba ones, being given by the substitutions indicated in the second square brackets.

The single-particle states of the noninteracting Hamiltonian (2), $H\psi_a = \epsilon_a\psi_a$, are computed as eigenvalues and eigenvectors of the matrices (3)–(5), $\psi_a(r_k,\varphi_j) = \sum_\sigma \Psi_{a,\sigma}(k,j)|\sigma\rangle$, where $\Psi_{a,\sigma}(k,j)$ are c numbers. The implicit boundary condition is that $\psi_a \equiv 0$ everywhere outside the ring, i.e., for $r < R_{\rm int}$ and $r > R_{\rm ext}$.

In the basis provided by $\{\psi_a\}$ the *interacting* many-body Hamiltonian is written in the second quantization as

$$\mathcal{H} = \sum_a \epsilon_a c_a^\dagger c_a + \frac{1}{2}\sum_{abcd} V_{abcd}c_a^\dagger c_b^\dagger c_d c_c, \quad (6)$$

where $c_a^\dagger$ and c_a are the creation and annihilation operators on the single-particle state a. The matrix elements of the Coulomb potential $V(\mathbf{r}-\mathbf{r}') = e^2/(\kappa|\mathbf{r}-\mathbf{r}'|)$, κ being the dielectric constant of the material, are in general give by

$$V_{abcd} = \langle\psi_a(\mathbf{r})\psi_b(\mathbf{r}')|V(\mathbf{r}-\mathbf{r}')|\psi_c(\mathbf{r})\psi_d(\mathbf{r}')\rangle. \quad (7)$$

In the present discrete model the double scalar product is in fact a double summation over all the lattice sites and spin labels,

$$V_{abcd} = Tt_C\sum_{\substack{kj\sigma\\k'j'\sigma'}}\Psi_{a,\sigma}^*(kj)\Psi_{b,\sigma'}^*(k'j')\frac{R_{\rm ext}}{|\mathbf{r}_{jk}-\mathbf{r}_{j'k'}|} \times \Psi_{c,\sigma}(kj)\Psi_{d,\sigma'}(k'j'). \quad (8)$$

The new energy parameter introduced by the Coulomb repulsion is $t_C = e^2/(\kappa R_{\rm ext}T)$. In the above summation over the sites, the contact terms ($k = k', j = j'$) are avoided, as their contribution vanishes in the continuous limit.

The many-body states Φ_μ are found by solving the eigenvalue problem for the Hamiltonian (6),

$$\mathcal{H}\Phi_\mu = E_\mu\Phi_\mu.$$

A potential solution of the equation is written in the configuration-interaction representation[13–15] as a linear

combination of the noninteracting system eigenstates (Slater determinants),

$$\Phi_\mu = \sum_A c_{\mu A}|A\rangle, \tag{9}$$

with $\{|A\rangle = |i_1^A, i_2^A, \ldots, i_K^A\rangle\}$ where $i_a^A = 0,1$ is the occupation number of the single-particle state ψ_a and K is the number of single-particle states considered. The occupation numbers i_K^A are listed in increasing energy order, so ϵ_K is the highest energy of the single-particle state included in the many-body basis. For any $|A\rangle$ we have $\sum_a i_a^A = N$, which is the number of electrons in the ring. It is straightforward to derive the matrix elements of $\mathcal{H}_{AA'}$ using the action of the creation and annihilation operators on the many-body basis. In practice, Eq. (9) is convergent with K for a sufficiently small number of electrons and sufficiently small ratio of Coulomb to confinement energy, t_C. This procedure, also known as "exact diagonalization," does not rely on any mean-field description of the Coulomb effects, like Hartree, Hartree-Fock, or density functional theory.[16]

To be able to carry out the numerical calculations in a reasonable amount of time, we choose a small ring of radii $R_{\text{ext}} = 50$ nm and $R_{\text{int}} = 0.8R_{\text{ext}}$, containing $N \leqslant 4$ electrons. The discretization grid has 10 radial and 50 angular points (500 sites), as shown in Fig. 1. Two common semiconductor materials used in the experimental spintronics are used for the selection of the material constants needed: InAs with $m^* = 0.023m_e$, $g^* = -14.9$, $\kappa = 14.6$, and estimated (or possible) values for the spin-orbit interactions $\alpha \approx 20$ and $\beta \approx 3$ meV nm; InSb with $m^* = 0.014m_e, g^* = -51.6, \kappa = 17.9$, and $\alpha \approx 50$, $\beta \approx 30$ meV nm.[4,5] The relative energies which we defined are as follows: for InAs $t_\alpha = 0.60$, $t_\beta = 0.09$, $t_C = 2.9, \gamma = -0.17$; for InSb $t_\alpha = 0.92$, $t_\beta = 0.55$, $t_C = 1.5, \gamma = -0.36$. In our calculations we have considered material parameters somewhere in between these two sets: $t_\alpha = 0.7$, $t_\beta = 0.3$, $t_C = 2.2, \gamma = -0.2$.

III. RESULTS

A. Single-particle calculations

In the absence of the SOI ($\alpha = \beta = 0$), the single-particle Hamiltonian (2) shares its eigenstates ψ_a with the $\hat{z}$ components of the angular momentum L_z and spin $S_z = \hbar\sigma_z/2$. In the presence of only one type of SOI, either $\alpha \neq 0$ or $\beta \neq 0$, the Hamiltonian commutes with the $\hat{z}$ component of the total angular momentum, $L_z + S_z$, which is conserved. When both $\alpha \neq 0$ and $\beta \neq 0$, the angular momentum is no longer conserved. However, ψ_a continue to be eigenstates of the parity operator $\mathcal{P} = \Pi\sigma_z$, Π being the (three-dimensional) spatial inversion operator. Indeed, the general Hamiltonian (2) commutes with $\mathcal{P}$, which can be easily verified by using $\Pi\mathbf{p} = -\mathbf{p}\Pi$ and the commutation rules of the Pauli matrices. So in general $\mathcal{P}\psi_a = s\psi_a$, and thus the parity $s = \pm 1$ of any state a is conserved, i.e., it is independent of the magnetic field. In particular, when $\alpha = \beta$ and $g^* = 0$, all states become parity degenerate at any magnetic field.[8,10,17] We identify the parity of the single-particle states calculated on our discrete ring model by looking at the relation $\psi_{a,\sigma}(k,j) = s\sigma\psi_{a,\sigma}(k,\bar{j})$, where (k,j) and $(k,\bar{j})$ are diametrically opposed sites, with angular coordinates $\varphi_{\bar{j}} = \varphi_j + \pi$.

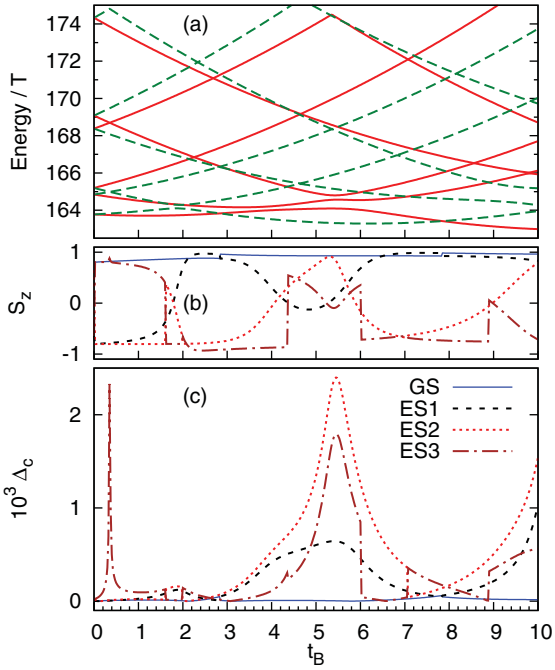

FIG. 2. (Color online) (a) The lowest 12 energies of the single-particle states vs the magnetic energy t_B. The solid (red) and the dashed (green) lines show the states with positive and negative parity, respectively. (b) The expected value of the spin projection along the z direction, S_z, in units of $\hbar/2$, for the first four states on the energy scale. (c) The standard deviation Δ_c of the charge distribution around the circle with radial site index $k = 6$, for the first four energy states: ground state (GS), first, second, and third excited states (ES1, ES2, and ES3). The same association of line types with states is used in (b).

In Fig. 2 we show the single-particle-state energy for $0 < t_B < 10$ (units of T), which corresponds to a magnetic field strength between 0 and 1.32 Tesla. Further increment of the magnetic field requires an augmentation of the number of sites on the ring in order to maintain the discrete model as a reasonable approximation of a physically continuous ring. The displayed results change by less than 1% if the number of sites increases, for example, from 500 to 600. At zero magnetic field all states are parity degenerate, which is just the ordinary spin degeneracy. The degeneracy is in general lifted by a finite magnetic field. There are, however, some particular values of t_B where the degeneracy persists. This situation is represented in Fig. 2(a) by all intersection points of two lines corresponding to the two possible parities. Such intersections do not occur between states with the same parity. Due to the spin-orbit coupling, the orbital momentum of one state depends on the spin of the other state and vice versa, and, consequently, states of the same parity do in fact interact and thus avoid intersections.[10] Although in Fig. 2(a) many states represented by the same line type apparently cross each other, in reality there are always tiny gaps between them, similar to those visible at $t_B \approx 2$ between the first and the second excited states or at $t_B \approx 5.5$ between the first, second, and third excited states. The magnitude of these gaps depends on the g factor, reducing in size for a smaller g^* parameter.

In Fig. 2(b) the evolution of the expected spin in the z direction, $S_z = \hbar\langle\psi_a|\sigma_z|\psi_a\rangle/2$, is presented for the first four states in the energy order. One can see how the spin flips for states avoiding the crossing, like those with negative parity at $t_B \approx 2$ [dashed and dotted lines in Fig. 2(b)].

Only one type of SOI, either Rashba or Dresselhaus, is sufficient to avoid the crossing of states with the same parity, but in this case the charge and the spin densities are uniform around the ring. When *both* SOI types are present the charge and spin densities become nonuniform. This situation is equivalent to the presence of a potential with two maxima and two minima around the ring, having reflection symmetry relative to the axes $y = x$ (or $\varphi = \pi/4$, corresponding to the crystal direction [110]) and $y = -x$ (or $\varphi = -\pi/4$, corresponding to the crystal direction $[1\bar{1}0]$).[8,10] The amplitude of the CDD is illustrated in Fig. 2(c) where the standard deviation (in the statistical sense) Δ_c of the charge density calculated around one circle on the ring, close to the mean radius, with radial site index $k = 6$, is plotted for the four lowest-energy states. The density deformation occurs on account of the two combined SOI types which lead to spin interference and additional interaction between states with the same parity. Consequently, the amplitude of the CDD for a certain state is maximum at those magnetic fields where the parity degeneracy is lifted (the state avoids a crossing with another state of the same parity). In Fig. 2(c) this is clearly seen at $t_B \approx 2$ for the excited state. In this example the CDD in the ground state is very weak. The sharp peak at $t_B \approx 0.4$ indicates the existence of a narrow gap between the fourth and fifth energy states that avoid crossing.

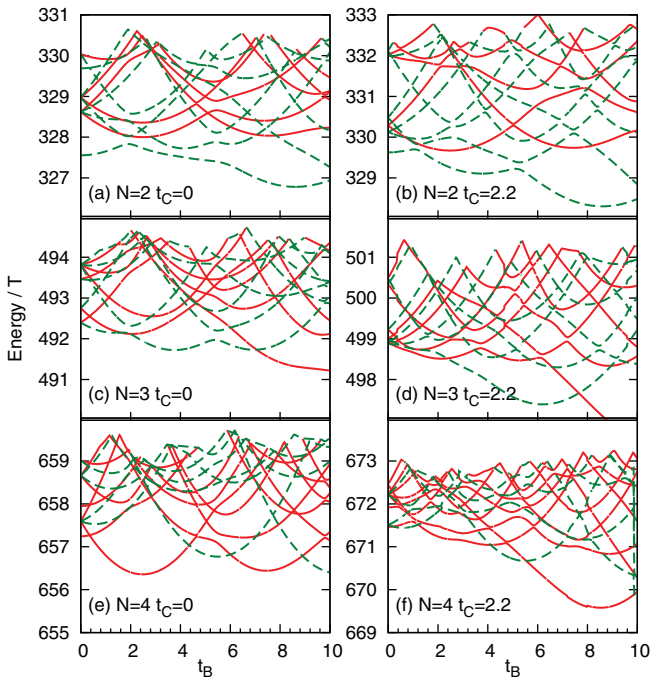

FIG. 3. (Color online) Energy spectra of the first 12 states for $N = 2$, 3, and 4 electrons without Coulomb interaction, $t_C = 0$, in (a),(c),(e), and with Coulomb interaction, $t_C = 2.2$, in (b),(d),(f). The solid (red) and the dashed (green) lines show the states with positive and negative parity, respectively.

B. Many-particle calculations

In the following considerations, we will include more than one electron. In Fig. 3 we compare the energy spectra for the first 12 many-body states vs the magnetic energy, for $N = 2$, 3, and 4 electrons, without and with Coulomb interaction. The number of single-particle states used to calculate the spectra with interaction varied between $K = 12$ and 14, the results being convergent within less than 1%. Since the Coulomb interaction is invariant at spatial inversion (and independent of spin) the parity s is also conserved in the many-body states. Spectra drawn for $t_C = 0$ and $t_C = 2.2$ have qualitatively similar features. To allow the comparison of the noninteracting and interacting spectra, we used on the horizontal axes exactly the same values of the magnetic energy and on the vertical axes different energy intervals, but with the same length. The interacting spectra present a shift to higher energies, on account of the additional Coulomb energy. Moreover, the crossings and the anticrossings of the energy levels (the points where the crossings were avoided) occur at different magnetic fields.

The total spin S_z for each of the first three energy states is shown in Fig. 4. At zero magnetic field, for an even number of electrons, here $N = 2$ or 4, the ground state is nondegenerate and has total spin $S_z = 0$, i.e., the spin-up and spin-down states of individual electrons compensate. For $N = 3$ the ground state is spin (doubly) degenerate at zero field. When the field is applied, the first spin flip in the interacting ground state, as well as the spin saturation, occur at lower magnetic fields than in the absence of the Coulomb repulsion. This is a result of

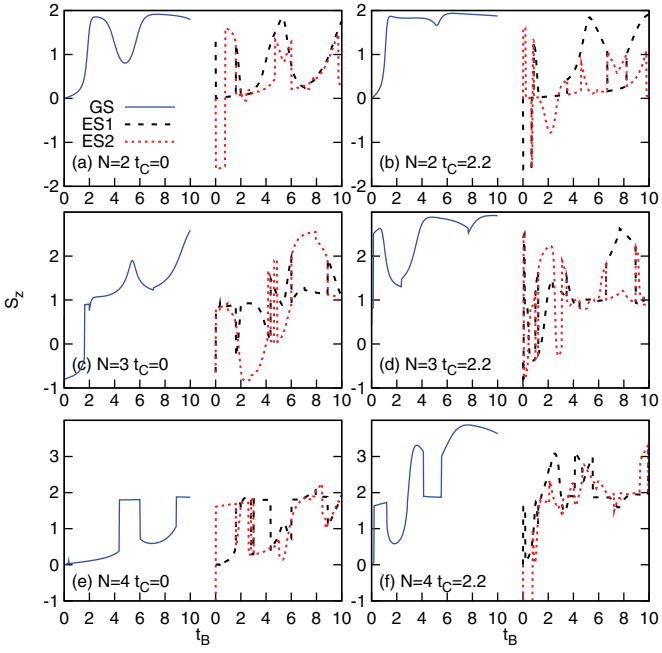

FIG. 4. (Color online) The total spin projection in the z direction, in units of $\hbar/2$, for the many-body states with $N = 2,3,4$ electrons, without interaction, i.e., $t_C = 0$, in (a),(c),(e), and with interaction, with $t_C = 2.2$, in (b),(d),(f). Only the first three states are shown here, the ground state (GS), the first excited state (ES1), and the second excited state (ES2). The magnetic energy t_B varies between 0 and 10 and the dashed lines, showing the excited states, are shifted to the right for clarity.

the mixing of spin states with the same parity produced by the interaction. This effect might also be related to the Coulomb exchange enhancement of the g factor obtained in the Hartree-Fock approximation for quantum dots,[18] although with about 20 electrons or more, and also to the similar enhancement of the SOI known in the homogeneous two-dimensional electron gas.[19] However, since here we have only up to four electrons, this comparison remains only qualitative.

As for noninteracting electrons (Fig. 2) abrupt or (relatively) smooth spin transitions occur with increasing magetic field, depending on whether the energy levels have crossings or anticrossings. Such transitions may repeat back and forth, resulting in sharp peaks of S_z, seen for example in Fig. 4(b) or 4(c).

As in the case of one electron ($N = 1$, Fig. 2), the charge deformation of each state is maximized for those magnetic fields where the state has an anticrossing (or repulsion) with another state of the same parity. The charge deformation parameter Δ_c is shown in Fig. 5. For $N = 2$ the amplitude of the CDD increases with the Coulomb interaction. There is a simple reason for that: the potential associated with the charge deformation has two minima diametrically opposite each other on the ring, and each of the two electrons tends to be localized in one of these minima. The mutual Coulomb repulsion fixes the electrons in those places better.[9,10] The situation changes, however, for $N > 2$. The Coulomb forces spread the electrons differently, more or less uniformly, such that the charge deformation created by the SOI is drastically reduced. In other words, the associated potential is strongly screened even by one extra electron above $N = 2$. This effect can be clearly seen in Fig. 5, comparing Fig. 5(c) with 5(d) and 5(e) with 5(f). The vertical scale of Figs. 5(d) and 5(e) has been magnified three times, for visibility.

In principle, the screening of the charge deformation is not particularly related to the spin-orbit effects. SOI only generates the specific effective potential which determines the CDD. In the absence of SOI ($\alpha = \beta = 0$), we checked that a similar screening effect occurs in the presence of a potential that induces a charge deformation comparable to that obtained with the SOI. It is, however, surprising that by adding only one extra electron such a drastic effect ensues.

Next, we investigate the effect of the Coulomb interaction on the spin distribution around the ring. The standard deviation of the spin density projected along the z direction, Δ_z, is plotted in Fig. 6, where we show the results calculated as before for the circle corresponding to the sites with radial coordinate $k = 6$. The spin density deformation is actually amplified by the Coulomb interaction for all $N = 2,3,4$. Like the CDDs, the SDDs reach their maxima at the magnetic fields where level repulsion occurs and remains prominent even when the gaps are very small. The Coulomb amplification is a result of the mixing of states with the same parity, but with different spin

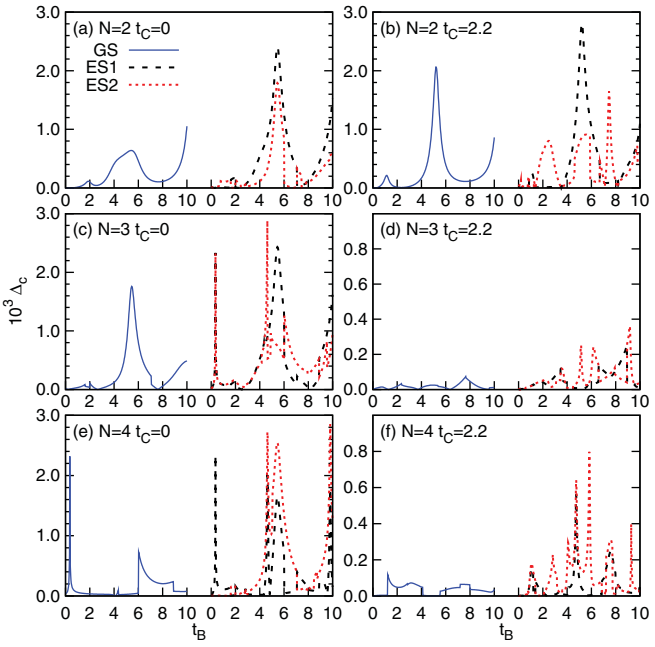

FIG. 5. (Color online) The standard deviation Δ_c of the charge on the circle $k = 6$ around the ring, as a measure of the amplitude of the charge deformation. Shown are the results for the ground state (GS), the first excited state (ES1), and the second excited state (ES2), for $N = 2,3,4$ electrons without ($t_C = 0$) and with ($t_C = 2.2$) interaction. The amplitude of the CDDs is strongly reduced by the Coulomb effects for $N = 3,4$; notice the different scales used in the paired panels (c),(d) and (e),(f). The magnetic energy t_B varies between 0 and 10 and the dashed lines, corresponding to the excited states, are shifted to the right for clarity. The sharp peaks correspond to narrow gaps in the energy spectra shown in Fig. 3 and the broader peaks to wider gaps.

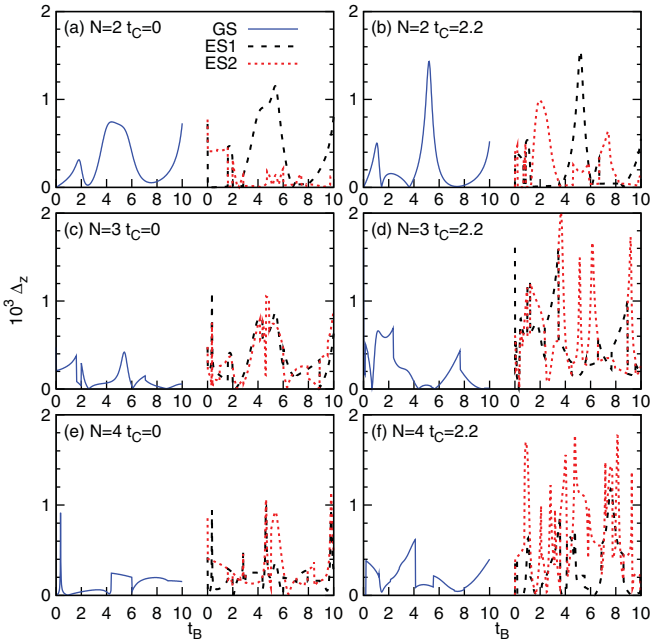

FIG. 6. (Color online) The standard deviation Δ_z of the spin projection along the z direction on the circle $k = 6$ around the ring, as a measure of the amplitude of the spin density wave. As in the previous figures, GS, ES1, and ES2 in the legend indicate the ground state, the first excited state, and the second excited state, respectively. The results are shown for $N = 2,3,4$ electrons without ($t_C = 0$), and with ($t_C = 2.2$) interaction. Unlike the CDDs, the SDDs are amplified by the Coulomb interactions for all N. The magnetic energy t_B varies between 0 and 10, and the dashed lines, corresponding to the excited states, are shifted to the right for clarity.

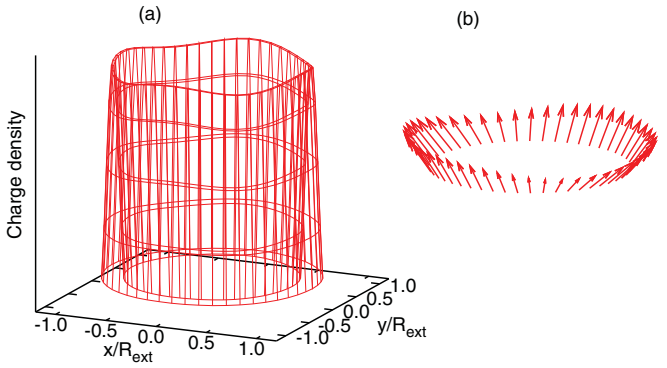

FIG. 7. (Color online) (a) The charge density for $N = 4$ electrons with interaction ($t_C = 2.2$), in the second excited state, i.e., ES2 in Fig. 5(f), with magnetic energy energy $t_B = 4.5$. (b) The corresponding total spin distribution along the ring $k = 6$ where the standard deviation of the z component is calculated and shown in Fig. 6(f).

orientations produced by the Coulomb potential. Consequently the SDDs have in general a richer structure than the CDDs.

Finally, in Fig. 7 we display an example of CDD and SDD, obtained for $N = 4$ interacting particles. The charge and spin distributions correspond to the second excited state and $t_B = 4.5$, the deformations being shown in Figs. 5(f) and 6(f), respectively. The CDD is weak, but still it has four visible maxima. For two electrons the CDD has only two maxima which are along the directions $x = y$ or $x = -y$, depending on the state and on the magnetic field, both with and without the Coulomb interaction. In particular, for a strictly one-dimensional ring model and $N = 2$, in the ground state, the maxima are always along the line $x = -y$,[8,9] whereas for a two-dimensional model they can also be along $x = y$.[10] But in general, for $N > 2$ electrons, screening effects may distribute the charge in more complicated configurations. Similar profiles with multiple local oscillations may be obtained for the spin density, eventually becoming spin density waves around the ring.[8]

IV. CONCLUSIONS

We calculated the many-body states of a system of $N = 2$, 3, and 4 interacting electrons located in a ring of finite width with Rashba and Dresselhaus spin-orbit coupling, in the presence of a magnetic field perpendicular to the surface of the ring. The Coulomb effects are fully included in the calculation via the exact diagonalization method. We obtained inhomogeneous charge densities, or CDDs, around the ring due to the combined effect of the two types of SOI. When the Coulomb interaction is included the charge deformation is amplified for $N = 2$, as also shown by other authors.[9,10] For $N > 2$ we find that the CDD is dramatically flattened out in the presence of the Coulomb interaction. We interpret the result as a screening effect. In contrast, the spin inhomogeneities, or SDDs, are amplified by Coulomb effects for all $N > 1$.

ACKNOWLEDGMENTS

This work was supported by the Icelandic Research Fund. Valuable discussions with Sigurdur Erlingsson, Gunnar Thorgilsson, and Marian Niţă are cordially acknowledged.

[1] S. Datta and B. Das, Appl. Phys. Lett. **56**, 665 (1990).
[2] Y. A. Bychkov and E. I. Rashba, Pisma Zh. Eksp. Teor. Fiz. **46**, 66 (1984) [JETP Lett. **39**, 78 (1984)].
[3] G. Dresselhaus, Phys. Rev. **100**, 580 (1955).
[4] R. Winkler, *Spin Orbit Coupling Effects in Two-Dimensional Electron and Hole Systems* (Springer-Verlag, Berlin, 2003).
[5] T. Ihn, *Semiconductor Nanostructures: Quantum States and Electronic Transport* (Oxford University Press, Oxford, 2010).
[6] J. Splettstoesser, M. Governale, and U. Zülicke, Phys. Rev. B **68**, 165341 (2003).
[7] S. Souma and B. K. Nikolić, Phys. Rev. B **70**, 195346 (2004).
[8] J. S. Sheng and K. Chang, Phys. Rev. B **74**, 235315 (2006).
[9] Y. Liu, F. Cheng, X. J. Li, F. M. Peeters, and K. Chang, Phys. Rev. B **82**, 045312 (2010).
[10] M. P. Nowak and B. Szafran, Phys. Rev. B **80**, 195319 (2009).
[11] F. E. Meijer, A. F. Morpurgo, and T. M. Klapwijk, Phys. Rev. B **66**, 033107 (2002).
[12] The first and second derivatives of any generic function $f(x)$ are approximated as $f'(x) \approx [f(x+h) - f(x-h)]/h$ and $f''(x) \approx [f(x+h) + f(x-h) - 2f(x)]/h^2$, respectively, where h is considered sufficiently small.
[13] P. Hawrylak and D. Pfannkuche, Phys. Rev. Lett. **70**, 485 (1993).
[14] N. T. T. Nguyen and F. M. Peeters, Phys. Rev. B **83**, 075419 (2011).
[15] N. T. T. Nguyen and F. M. Peeters, Phys. Rev. B **78**, 045321 (2008).
[16] D. Pfannkuche, V. Gudmundsson, and P. A. Maksym, Phys. Rev. B **47**, 2244 (1993).
[17] J. Schliemann, J. C. Egues, and D. Loss, Phys. Rev. Lett. **90**, 146801 (2003).
[18] V. Gudmundsson and J. J. Palacios, Phys. Rev. B **52**, 11266 (1995).
[19] G.-H. Chen and M. E. Raikh, Phys. Rev. B **60**, 4826 (1999).